Supporting Information

Mass Transfer through Vapor-Liquid Interfaces studied by Non-Stationary Molecular Dynamics Simulations

Dominik Schaefer,[1] *Simon Stephan,*[*,1] *Kai Langenbach,*[2]

Martin T. Horsch,[3] *and Hans Hasse*[1]

[1)]Laboratory of Engineering Thermodynamics (LTD), TU Kaiserslautern, 67663 Kaiserslautern, Germany

[2)]Institute of Chemical Engineering, University of Innsbruck, 6020 Innsbruck, Austria

[3)]Norwegian University of Life Sciences, Faculty of Science and Technology, Department of Data Science, Drøbakveien 31, 1430 Ås, Norway

[*]Corresponding author: simon.stephan@mv.uni-kl.de

Thursday 9th March, 2023

The Supporting Information for the publication "*Mass Transfer through Vapor-Liquid Interfaces studied by Non-Stationary Molecular Dynamics Simulations*" contains:

- Figure S.1: Details on the statistics of two sets of replicas at $T = 0.715\,\varepsilon k_\mathrm{B}^{-1}$.
- Details on the determination of the interface position and thickness.
- Figures S.2, S.3, and S.4: Pressure, density, and flux sampled in the measurement volumes as a function of time at the temperatures $T = 0.66, 0.77, 0.825\,\varepsilon k_\mathrm{B}^{-1}$. The results at $T = 0.715\,\varepsilon k_\mathrm{B}^{-1}$ are shown in the main work of the publication.
- Figure S.5: Pressure-composition diagrams as a function of time at the temperatures $T = 0.66, 0.77, 0.825\,\varepsilon k_\mathrm{B}^{-1}$. The results at $T = 0.715\,\varepsilon k_\mathrm{B}^{-1}$ are shown in the main work of the publication.
- Figures S.6, S.7, and S.8: Response of the system at the vapor-liquid interfaces for simulations at temperatures $T = 0.66, 0.77, 0.825\,\varepsilon k_\mathrm{B}^{-1}$ for both mixtures. The results at $T = 0.715\,\varepsilon k_\mathrm{B}^{-1}$ are shown in main work of the publication.

Details on the Statistics of a Set of Replicas

The initial number of particles and their initial configuration, the box size as well as the temperature were the same for all simulations in a set of replicas. The simulations from a set of replicas differ only in the initial velocities of the particles in the box at the beginning of the simulation. The initial velocity of each particle is randomly drawn from the Maxwell-Boltzmann distribution by using a random number generator. This ensures that the simulations from a set of replicas pass different trajectories in the phase space and representative and significant measures can be obtained from the simulations.

The stochastic nature of the Grand Canonical Monte Carlo algorithm utilized in the simulation method results in the fact that the number of inserted particles in the *In* phase differs among the simulations of a set of replicas. The variation of the number of inserted particles

in a set of replicas and its influence on observables is briefly discussed here. Figure S.1 shows the results from a set of replicas from mixtures A and one from mixtures B at $T = 0.715\,\varepsilon k_\mathrm{B}^{-1}$. The distribution of simulations, the density $\rho'_{2,\,\mathrm{Eq2}}$ and the delay time $\Delta\tau_\mathrm{d}$ as functions of the number of inserted particles N_2 are shown. The number of simulations with a certain number of inserted particles (cf. Figure S.1 (a)) shows that the distribution approximately follows a Gaussian distribution. For both mixtures the peak of the distribution is at about 1,200 and the scattering lies in the range 1,075 to 1,425. The standard deviation of the distributions is 46 for mixtures A and 64 for mixtures B. Hence, the set of replicas from mixtures B has a slightly broader distribution of the number of inserted particles compared to mixtures A.

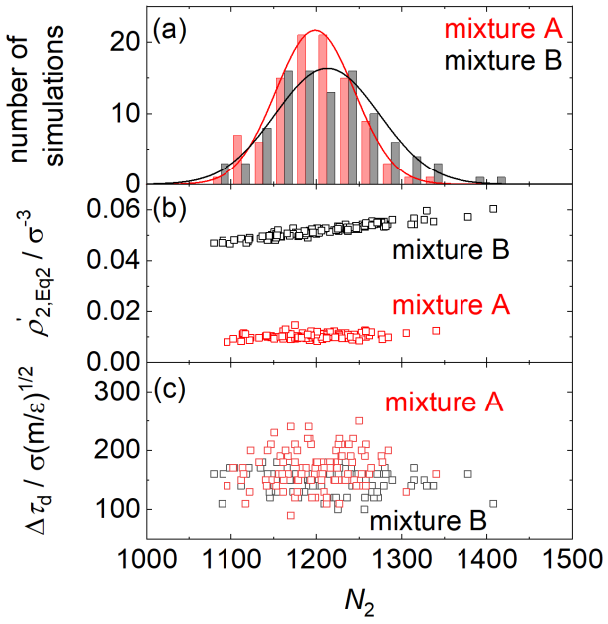

Figure S.1: Statistics from two exemplar sets of replicas with 100 simulations each: One for mixtures A (red) and one for mixture B (black) at $T = 0.715\,\varepsilon k_\mathrm{B}^{-1}$. Histogram of the number of simulations (top), density of component 2 at equilibrium state *Eq2* $\rho'_{2,\,\mathrm{Eq2}}$ in the measurement volume in the liquid phase MV_liq (middle), and the delay time $\Delta\tau_\mathrm{d}$ (bottom) as functions of the number of inserted particles N_2. Red and black lines in the top represent Gaussian distribution functions fitted to the respective data.

Figure S.1 (b) shows that the variation of N_2 has only a minor influence on the density $\rho'_{2,\,\mathrm{Eq2}}$ in the equilibrium state after the relaxation process of component 2 in the liquid phase

measurement volume $\mathrm{MV_{liq}}$. For mixtures B, a tendency can observed that $\rho^{'}_{2,\,\mathrm{Eq2}}$ slightly increases with increasing N_2, which is simply due to the fact that a slightly different state point of the binary mixtures is obtained if more component 2 particles are inserted. The density $\rho^{'}_{2,\,\mathrm{Eq2}}$ obtained for mixtures B is stronger influenced by N_2 than mixtures A, since the majority of inserted component 2 particles end up in the liquid phase in the equilibrium *Eq2* in the case of mixtures B. This is simply a result of the large differences in the gas solubility of the two mixtures.[1,2]

The delay time $\Delta\tau_\mathrm{d}$ is defined as the time span between the start of the insertion phase at $\tau = 1\,000\,\sigma(m/\varepsilon)^{1/2}$ and the time at which the density of component 2 exceeds $\rho_2'(\tau) \geq 0.0001\,\sigma^{-3}$ in the liquid phase measurement volume. For both mixtures, the number of inserted particles N_2 has no significant influence on the delay time $\Delta\tau_\mathrm{d}$. Furthermore, the delay time is the same for both mixtures within the scattering, which is also seen in density response in the liquid phase in Figures S.2 (b),S.3 (b), and S.4 (b) and the corresponding Figure in the main work of this publication at $T = 0.715\,\varepsilon k_\mathrm{B}^{-1}$.

Overall, the scattering of the number of inserted particles N_2 within a set of replicas has a small effect on the response of the system. Thus, the method of set of replicas gives a clearer view of the dynamic processes within the system. The set of replicas helps to distinguish between physically relevant processes and noise.

Simulation Details: Determination of the Interface Position and Thickness

For the determination of the density $\rho^{'}$ and $\rho^{''}$ of the liquid and vapor bulk, first the z-position of the global minimum and maximum of the gradient $\partial\rho/\partial z$ is determined. The maximum is the initial guess for the position of the right interface, the minimum is the initial guess for the left interface. Based on the initial guesses of the interface position, the bulk density $\rho^{'}$ and $\rho^{''}$ are sampled in a distance of 1/3 of the size of the liquid phase in z-direction to the minimum and maximum position of the gradient $\partial\rho/\partial z(z)$ in the liquid

and vapor phase. Bulk density are averaged over a length of 1/3 of the size of the liquid phase in z-direction. With the bulk density $\rho^{'}$ and $\rho^{''}$, the position z_{10}, z_{50}, and z_{90} can be precisely determined as the position where the density corresponds to

$$\begin{aligned} \rho_{10} &= \rho^{''} + 0.1(\rho^{'} - \rho^{''}) \\ \rho_{50} &= \rho^{''} + 0.5(\rho^{'} - \rho^{''}) \\ \rho_{90} &= \rho^{''} + 0.9(\rho^{'} - \rho^{''}) \end{aligned} \tag{1}$$

Response in the Liquid and Vapor Phases for Various Temperatures

Figures S.2, S.3, and S.4 show pressure, density, and net flux sampled in the measurement volumes as a function of time at temperatures $T = 0.66, 0.77, 0.825\,\varepsilon k_{\mathrm{B}}^{-1}$. The results are qualitatively similar to the results shown for $T = 0.715\,\varepsilon k_{\mathrm{B}}^{-1}$. The negative net flux in the vapor phase observable, which is only observed for mixture A, decreases with increasing temperature, which can be attributed the enrichment that is known to decreases with increasing temperature.[1,2]

Figure S.5 shows the pressure as a function of composition and time at the temperatures $T = 0.66, 0.77, 0.825\,\varepsilon k_{\mathrm{B}}^{-1}$. Results sampled in the measurement volumes for both mixtures A and B are shown. For all studied temperatures, the vapor and liquid equilibrium state points of *Eq1* and *Eq2* obtained from the NEMD simulations are in good agreement with the results from the PeTS EOS.[3,4] Furthermore, in all studied cases, the vapor and liquid phase pressure are in excellent agreement – as expected in equilibrium. The pressure $p(x_2, \tau)$ sampled in the liquid and vapor phase follows a similar course over time as shown for $T = 0.715\,\varepsilon k_{\mathrm{B}}^{-1}$ in the main work of the publication for each mixture. In the case of mixture B, the pressure sampled in the vapor phase intersect the dew line for the first time at $1,200 \leq \tau / \sigma(m/\varepsilon)^{1/2} \leq 1,250$ at all temperatures. From the intersection point, the pressure and composition sampled in the measurement volume of the vapor phase follows the dew line towards *Eq2* at all temperatures.

The vapor phase of mixture B is close to equilibrium states but is continuously shifted out of equilibrium by the mass transfer in the liquid phase, which is observed at all temperatures. For mixture A, the pressure and composition sampled in the vapor phase first intersects the dew line at higher pressure and composition than *Eq2* state point with the exception of the results for $T = 0.825\,\varepsilon k_{\mathrm{B}}^{-1}$, for which the dew line is intersected at lower pressure and composition.

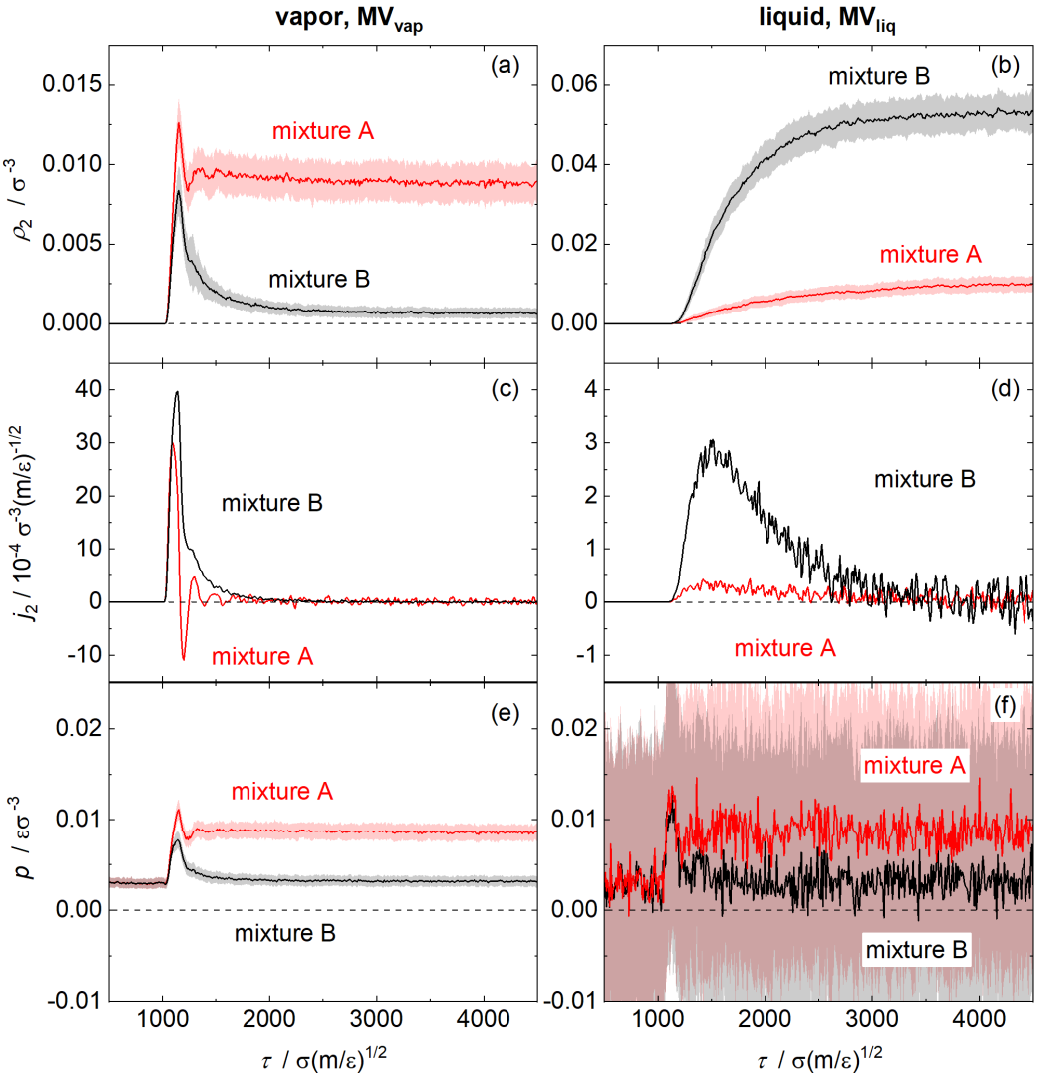

Figure S.2: Observables sampled in the replica NEMD simulations in the measurement volumes in the vapor phase $\mathrm{MV_{vap}}$ (left) and in the liquid phase $\mathrm{MV_{liq}}$ (right), respectively, as a function of the simulation time: density of component 2 ρ_2, flux of component 2 j_2, and pressure p. The temperature was $T = 0.66\,\varepsilon k_\mathrm{B}^{-1}$. Results for mixtures A are indicated in red; results for mixtures B in black. Solid lines indicate the mean value obtained from the set of replicas, the shaded area indicates standard deviation. The standard deviation is only given for the two properties that were sampled directly (ρ_2 and p); j_2 was calculated from ρ_2.

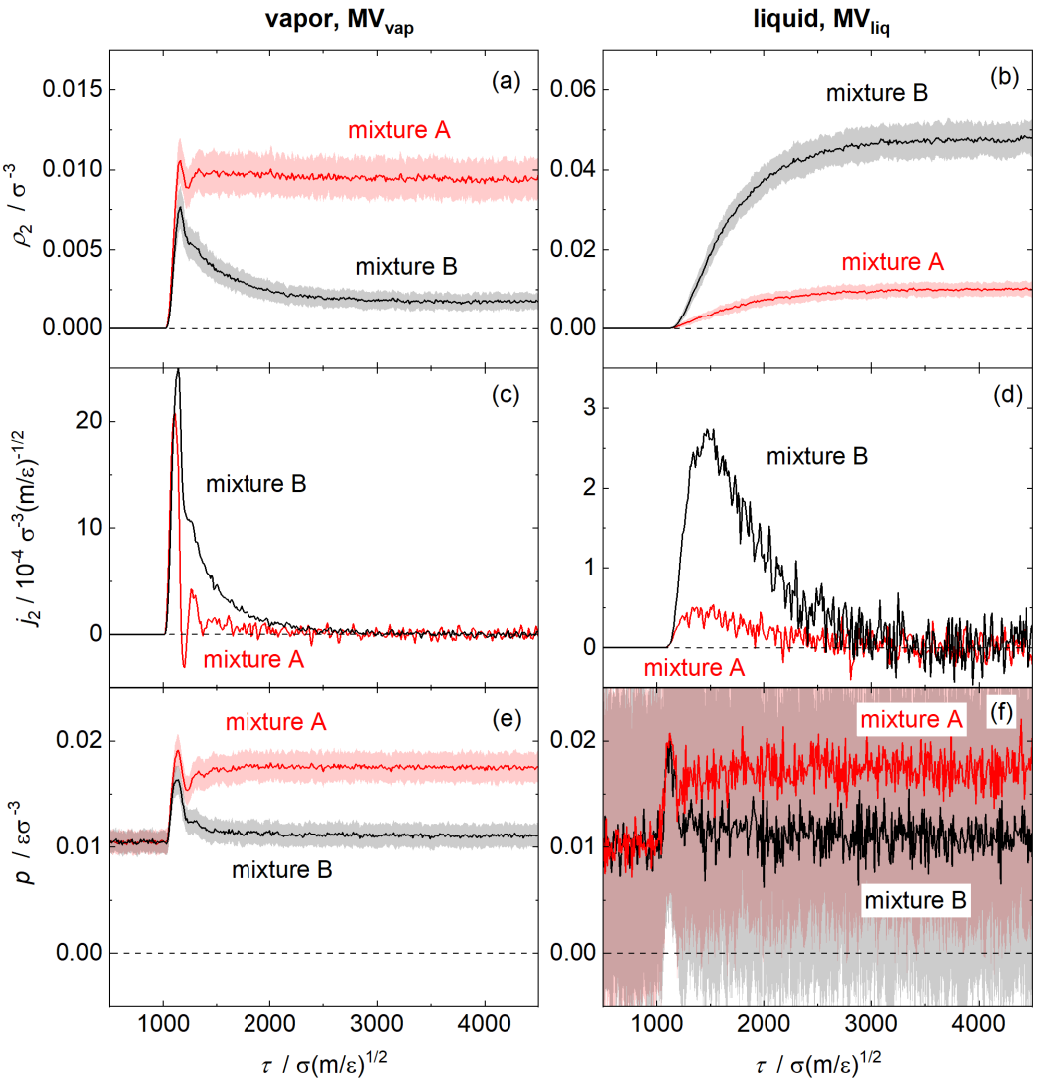

Figure S.3: Observables sampled in the replica NEMD simulations in the measurement volumes in the vapor phase $\mathrm{MV_{vap}}$ (left) and in the liquid phase $\mathrm{MV_{liq}}$ (right), respectively, as a function of the simulation time: density of component 2 ρ_2, flux of component 2 j_2, and pressure p. The temperature was $T = 0.77\,\varepsilon k_\mathrm{B}^{-1}$. Results for mixtures A are indicated in red; results for mixtures B in black. Solid lines indicate the mean value obtained from the set of replicas, the shaded area indicates standard deviation. The standard deviation is only given for the two properties that were sampled directly (ρ_2 and p); j_2 was calculated from ρ_2.

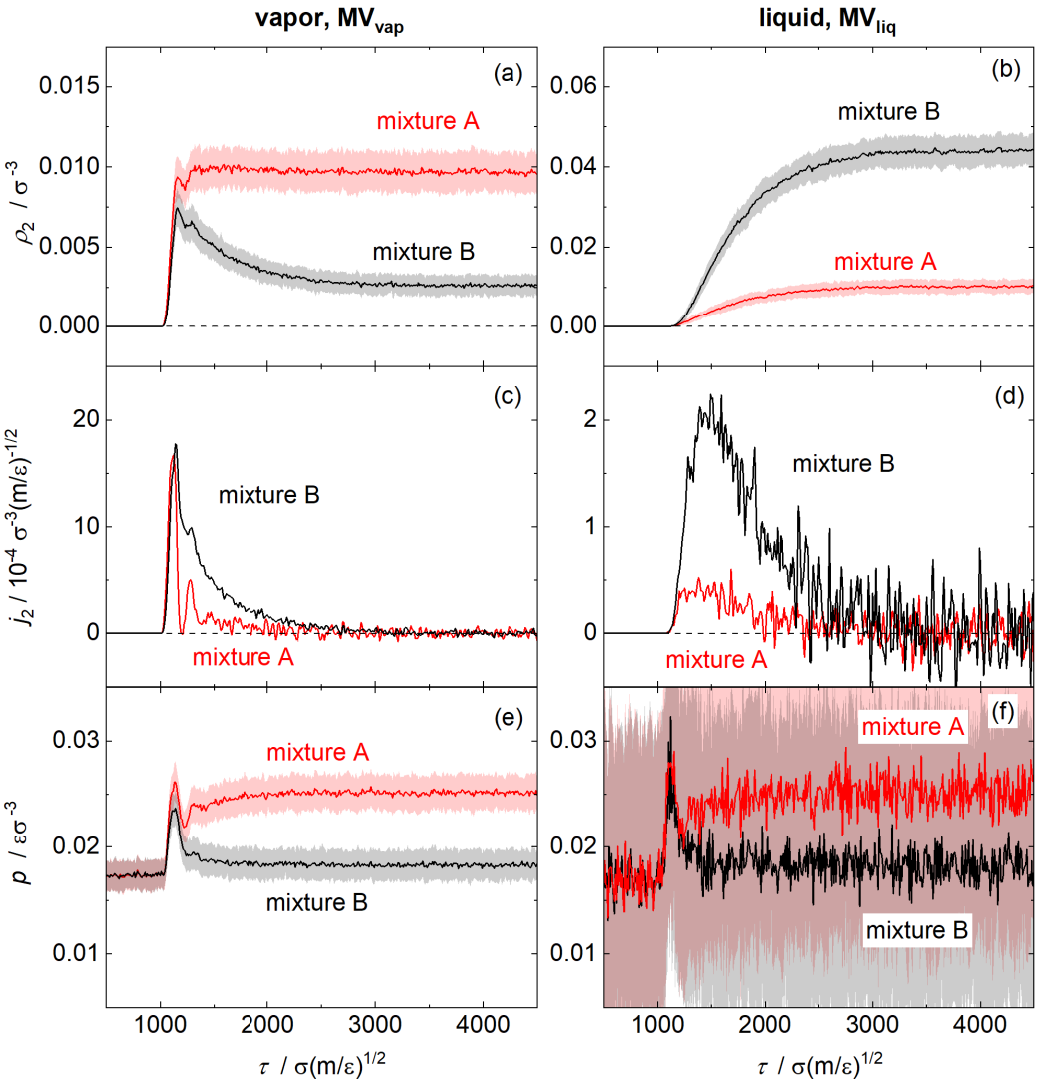

Figure S.4: Observables sampled in the replica NEMD simulations in the measurement volumes in the vapor phase $\mathrm{MV_{vap}}$ (left) and in the liquid phase $\mathrm{MV_{liq}}$ (right), respectively, as a function of the simulation time: density of component 2 ρ_2, flux of component 2 j_2, and pressure p. The temperature was $T = 0.825\,\varepsilon k_\mathrm{B}^{-1}$. Results for mixtures A are indicated in red; results for mixtures B in black. Solid lines indicate the mean value obtained from the set of replicas, the shaded area indicates standard deviation. The standard deviation is only given for the two properties that were sampled directly (ρ_2 and p); j_2 was calculated from ρ_2.

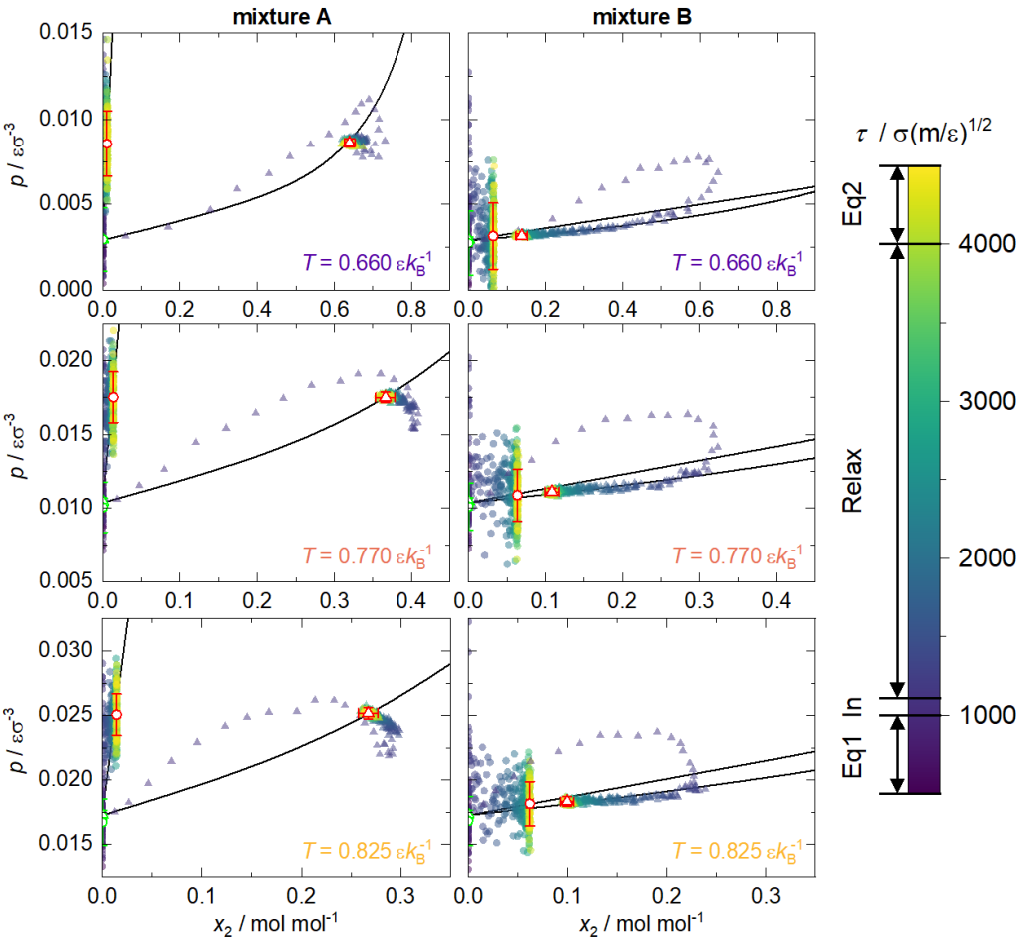

Figure S.5: Pressure-composition diagrams for mixtures A (left) and mixtures B (right). Results for at $T = 0.66\,\varepsilon k_\mathrm{B}^{-1}$ (top), at $T = 0.77\,\varepsilon k_\mathrm{B}^{-1}$ (middle), and at $T = 0.825\,\varepsilon k_\mathrm{B}^{-1}$ (bottom). Circles indicate state points sampled in the measurement volume $\mathrm{MV_{liq}}$; triangles indicate state points sampled in the measurement volume $\mathrm{MV_{vap}}$. The color scale indicates the simulation time. Each data point represents the mean value obtained from a set of replicas at a given simulation time τ. The white filled symbols indicate pressure and composition in *Eq1* (green) and in *Eq2* (red) phases. The error bars are the standard deviation obtained from a set of replicas. The black line indicates the phase equilibrium computed with the PeTS EOS.[3,4]

Response at the Vapor-Liquid Interface

Figures S.6, S.7, and S.8 show the response of the system in the interfacial region and the neighboring bulk phases for simulations at temperatures $T = 0.66, 0.77, 0.825\,\varepsilon k_\mathrm{B}^{-1}$ for both mixtures. The temporary density peak of component 2 at the interface of mixture B decreases in height with increasing temperature. At the highest temperature, it vanishes nearly completely. This can be explained by a lower mass transfer resistance in the interface and the liquid phase at higher temperatures in mixture B. For mixture A at all temperatures, the density of component 2 at the interface is reaching its equilibrium value very quickly ($\Delta\tau = 200\,\sigma(m/\varepsilon)^{1/2}$), immediately forming the characteristic symmetric enrichment peak.

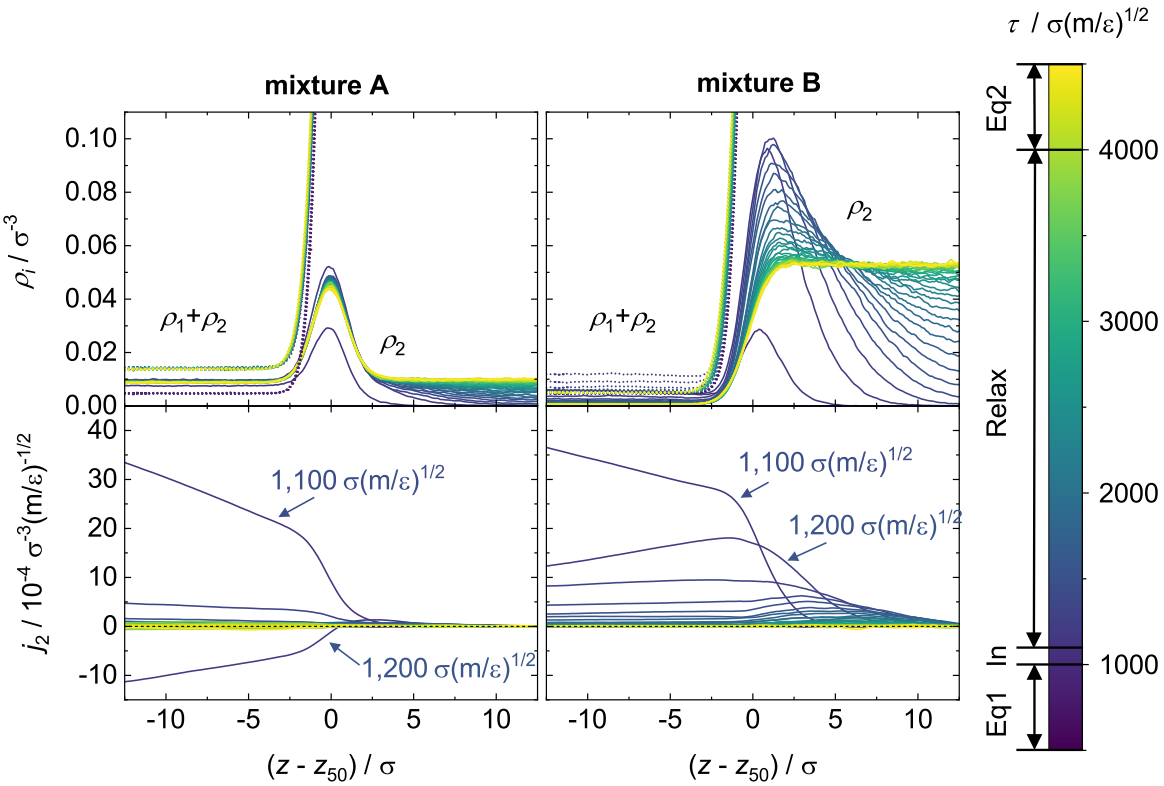

Figure S.6: Spatial profiles of the observables sampled in the vicinity of the interface and the neighboring bulk phases for mixture A (left) and mixture B (right). Results for the temperature $T = 0.66\,\varepsilon k_\mathrm{B}^{-1}$ from set of replicas. Top: density of the low-boiling component 2 (—) and total density (·····); Bottom: molar flux of component 2 j_2. The simulation time τ is indicated by the color. The shown profiles were measured at time intervals of $\Delta\tau = 100\,\sigma(m/\varepsilon)^{1/2}$.

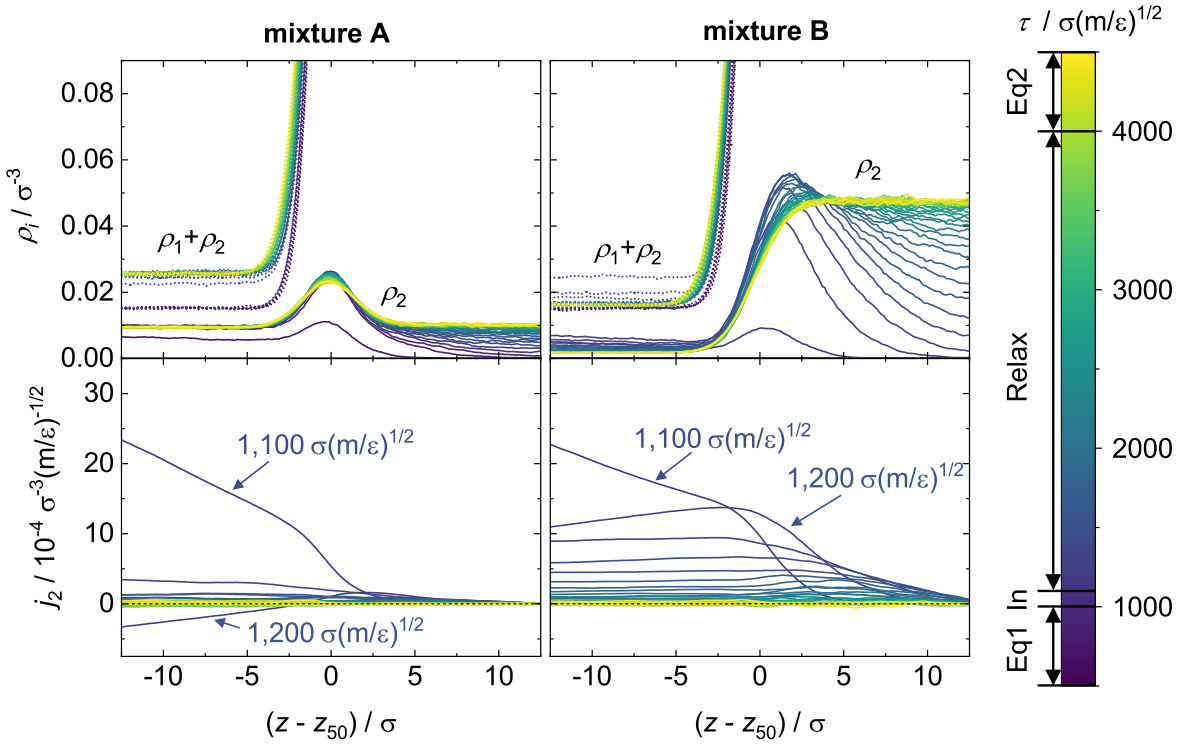

Figure S.7: Spatial profiles of the observables sampled in the vicinity of the interface and the neighboring bulk phases for mixture A (left) and mixture B (right). Results for the temperature $T = 0.77\,\varepsilon k_\mathrm{B}^{-1}$ from set of replicas. Top: density of the low-boiling component 2 (—) and total density (·····); Bottom: molar flux of component 2 j_2. The simulation time τ is indicated by the color. The profiles shown were measured at time intervals of $\Delta\tau = 100\,\sigma(m/\varepsilon)^{1/2}$.

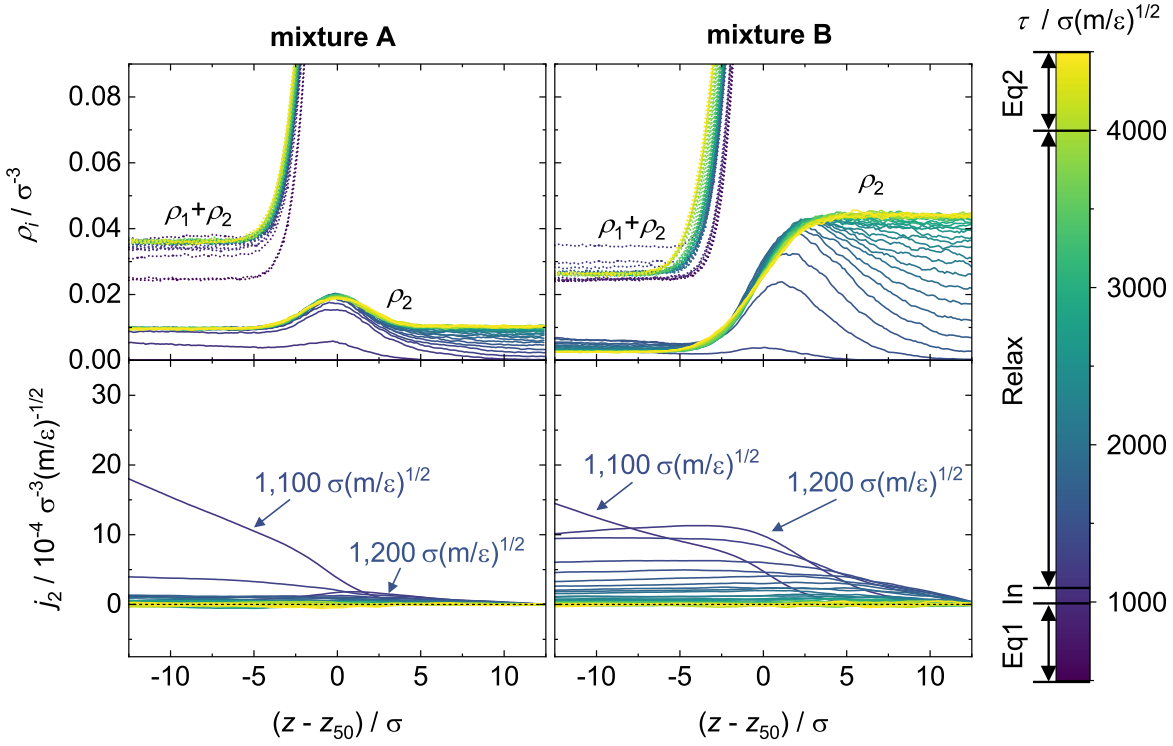

Figure S.8: Spatial profiles of the observables sampled in the vicinity of the interface and the neighboring bulk phases for mixture A (left) and mixture B (right). Results for the temperature $T = 0.825\,\varepsilon k_\mathrm{B}^{-1}$ from set of replicas. Top: density of the low-boiling component 2 (—) and total density (·····); Bottom: molar flux of component 2 j_2. The simulation time τ is indicated by the color. The profiles shown were measured at time intervals of $\Delta\tau = 100\,\sigma(m/\varepsilon)^{1/2}$.

References

(1) Stephan, S.; Hasse, H. Influence of Dispersive Long Range Interactions on Properties of Vapour-Liquid Interfaces of Binary Lennard-Jones Mixtures. *Molecular Physics* **2020**, *118*, e1699185.

(2) Stephan, S.; Hasse, H. Molecular interactions at vapor-liquid interfaces: Binary mixtures of simple fluids. *Physical Review E* **2020**, *101*, 012802.

(3) Heier, M.; Stephan, S.; Liu, J.; Chapman, W. G.; Hasse, H.; Langenbach, K. Equation of State for the Lennard-Jones Truncated and Shifted Fluid with a Cut-Off Radius of 2.5σ Based on Perturbation Theory and its Applications to Interfacial Thermodynamics. *Molecular Physics* **2018**, *116*, 2083–2094.

(4) Stephan, S.; Langenbach, K.; Hasse, H. Interfacial Properties of Binary Lennard-Jones Mixtures by Molecular Simulations and Density Gradient Theory. *The Journal of Chemical Physics* **2019**, *150*, 174704.